A two-step simulation methodology for modelling stagnation flame synthesised aggregate nanoparticles

Casper S. Lindberg[a,c], Manoel Y. Manuputty[a,c], Jethro Akroyd[a,c], Markus Kraft[a,b,c,*]

[a] *Department of Chemical Engineering and Biotechnology, University of Cambridge, Philippa Fawcett Drive, Cambridge, CB3 0AS, United Kingdom*
[b] *School of Chemical and Biomedical Engineering, Nanyang Technological University, 62 Nanyang Drive, 6357459, Singapore*
[c] *Cambridge Centre for Advanced Research and Education in Singapore (CARES), CREATE Tower, 1 Create Way, 138602, Singapore*

Abstract

A two-step simulation methodology is presented that allows a detailed particle model to be used to resolve the complex morphology of aggregate nanoparticles synthesised in a stagnation flame. In the first step, a detailed chemical mechanism is coupled to a one-dimensional stagnation flow model and spherical particle model solved using method of moments with interpolative closure. The resulting gas-phase profile is post-processed with a detailed stochastic population balance model to simulate the evolution of the population of particles, including the evolution of each individual primary particle and their connectivity with other primaries in an aggregate. A thermophoretic correction is introduced to the post-processing step through a simulation volume scaling term to account for thermophoretic transport effects arising due to the steep temperature gradient near the stagnation surface. The methodology is evaluated by applying it to a test case: the synthesis of titanium dioxide from titanium tetraisopropoxide (TTIP) precursor. The thermophoretic correction is shown to improve the fidelity of the post-process to the first fully-coupled simulation, and the methodology is demonstrated to be feasible for simulating the morphology of aggregate nanoparticles formed in a stagnation flame, permitting the simulation of quantities that are directly comparable to experimental observations.

Keywords: Stagnation flame, Population balance, Detailed particle model, Titanium dioxide, TTIP

*Corresponding author
Email address: mk306@cam.ac.uk (Markus Kraft)

1. Introduction

Combustion synthesis is a key route for nanoparticle production that has received significant focus in the research community. A common strategy to understand and optimize the synthesis process is to develop comprehensive models of the combustion system guided by experimental observations. In this paper, we develop a simulation methodology for modelling aggregate nanoparticles in a stagnation flame.

Premixed stagnation flame experiments have been used to synthesise and study nanoparticles, including ultra-fine titanium dioxide (titania, TiO_2) [1, 2, 3] and soot [4, 5]. The stagnation flame was introduced to avoid flame perturbations during sampling by embedding the sampling probe into the stagnation surface. Modelling is facilitated by this configuration since the probe may be treated as a boundary condition and a pseudo one-dimensional numerical solution to the flame becomes possible.

Various deterministic methods have been applied to solve the particle population dynamics with varying levels of detail in the particle description. These include moment methods [6, 7, 8] and sectional methods [9, 10, 11, 12, 13]. Moment methods are typically fast and easily coupled to gas-phase chemistry and flow dynamics, but do not resolve the particle size distribution (PSD). Sectional methods allow for some resolution of the PSD by dividing the distribution into a number of sections, but at greater computational expense. Both methods allow for some description of aggregate morphology. For example, Xiong and Pratsinis [9] presented a two-dimensional sectional technique that considered the surface area and volume of an aggregate particle, allowing sintering to be simulated. Often an assumption of monodisperse primary particles is made, though primary particle polydispersity has also been considered [13]. Moment methods have also been extended to model both particle surface area and volume [14, 15, 16, 17, 7], but like sectional methods these are generally limited to tracking two internal particle dimensions.

Nanoparticles formed in flames are often aggregates composed of polydisperse primary particles such as those shown in the transmission electron microscopy (TEM) image in Fig. 1. A detailed description of the aggregate particle morphology is therefore necessary to simulate quantities that are directly comparable with experimental observations. Menz and Kraft [18] emphasise the importance of selecting an appropriate model for the system being simulated, and warn of using an over-simplified model to interpret experimental data. Stochastic methods allow for the extension of the particle

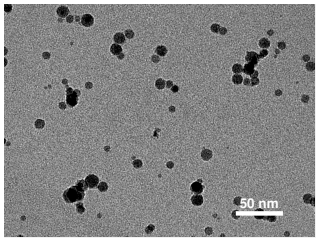

Figure 1: A typical experimental TEM image of stagnation flame synthesised TiO_2.

model to include a very detailed description of each particle and allow key physical details to be included, providing a powerful tool to investigate the mechanisms that control particle growth and morphology. Detailed particle models have been used to simulate soot [19], silicon [20], silica [21] and titania [22, 23].

Spatial inhomogeneity and flow dynamics, however, are not easily incorporated into models with a high-dimensional particle description. Instead of direct coupling, one approach has been to post-process existing flame data. This technique has been used successfully to simulate soot formation in premixed laminar flames with no stagnation surface [24, 25, 26, 27, 28]. Yapp et al. [19] applied the technique to model soot formation in a stagnation flame, but found that the simulations did not reproduce the experimental particle size distribution data well. While some of the differences can be attributed to uncertainties in the models used, the results also suggest that the post-processing methodology employed is unsuitable in cases with strong temperature gradients and significant thermophoretic transport effects.

The purpose of this paper is to present a two-step simulation methodology that allows a detailed particle model to be used to resolve the complex aggregate morphology of nanoparticles synthesised in a stagnation flame. The first step in the method couples detailed gas-phase chemistry, flow and a spherical particle model solved with method of moments with interpolative closure (MoMIC) to simulate the flame profile and particle moments. In the second step, the flame profile is post-processed with a very detailed particle model solved using a stochastic numerical method to resolve the aggregate particle morphology. We discuss how the steep temperature gradient at the stagnation surface requires the effect of thermophoresis to be accounted for in the post-processing step. To address this, we introduce a correction to the post-process through a modified simulation sample volume scaling term.

The simulation methodology is applied to the example of the combustion synthesis of TiO_2 nanoparticles from titanium tetraisopropoxide (TTIP) precursor. TiO_2 particles are an important industrial product and their func-

tionality is strongly influenced by the morphology and crystalline phase of the particles. A detailed particle description facilitates comparison with experimental observation such as TEM images and allows morphology dependent processes such as sintering and phase transformation to be studied. The methodology is evaluated by comparing results from both simulation steps for consistency. Finally, we simulate the stagnation flame experiment of Tolmachoff et al. [2] to demonstrate the ability of a detailed description of particles to provide additional insight into experimental results. The methodology presented in this paper is not dependent on the specific details of a particular particle model and can be applied to the study of various nanoparticles formed in stagnation flames.

2. Burner configuration

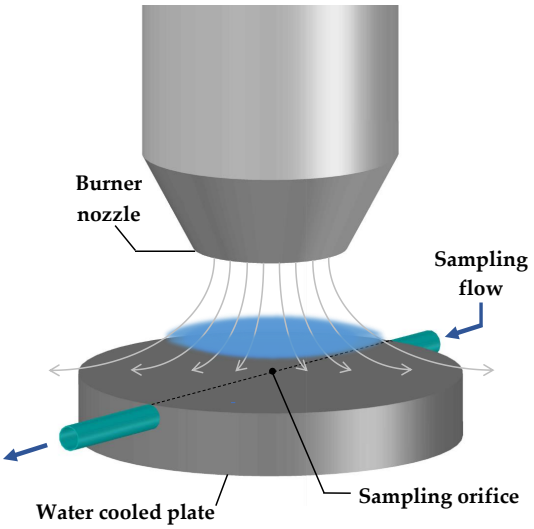

Figure 2: Schematic of experimental set-up being modelled.

A premixed laminar stagnation flame is modelled in this study. The set-up, shown in Fig. 2, is similar to that used in previous studies of titania and soot formation [2, 3, 29]. An aerodynamic nozzle issues a laminar jet of TTIP-doped premixed $C_2H_4/O_2/Ar$ that impinges on a water-cooled stagnation plate. A thin flame is formed and stabilised by stretch above the surface. Particles are sampled through an orifice at the centre of the plate.

3. Model description

3.1. Flow model

The flow is assumed to be an axisymmetric stagnation flow and is modelled using a pseudo one-dimensional approximation. This is described in detail by Manuputty et al. [8].

3.2. Chemical reaction model

The chemical model consists of a TTIP decomposition mechanism combined with hydrocarbon combustion chemistry described by the USC-Mech II model [30]. The TTIP decomposition model contains 25 Ti species and 65 reactions, and describes two of the main decomposition pathways identified by Buerger et al. [31]. The decomposition product for both pathways is titanium hydroxide ($Ti(OH)_4$), which is treated as the collision species for the particle inception and condensation reactions in the particle model.

3.3. Particle model

The mathematical description of a particle is called the type-space. In this work we use a spherical and a detailed type-space. The dynamics of the particle population are described by the Smoluchowski coagulation equation with additional terms for inception, condensation and sintering (detailed model only) [32]. A separate work with a comprehensive description of the detailed model type-space and particle processes is in preparation, so only a brief summary is given here.

3.3.1. Spherical particle model

The spherical particle model characterises a particle using its number of constituent TiO_2 monomers, i. The particle mass is $i \cdot m_{TiO_2}$, where m_{TiO_2} is the mass of a single monomer of TiO_2; and, assuming spherical geometry the particle diameter can be calculated. The collision limited inception and condensation processes are the same in both spherical and detailed particle models, and are outlined below. The particle models differ primarily in their treatment of a coagulation event: the spherical model effectively assumes instantaneous coalescence following the collision.

3.3.2. Detailed particle model

The type-space of the detailed particle model is illustrated in Fig. 3. An aggregate particle is composed of polydisperse primary particles modelled as overlapping spheres based on the approach of Eggersdorfer et al. [33, 34]. An aggregate particle containing $n_p(P_q)$ primary particles is represented as

$$P_q = P_q(p_1, ..., p_j, ..., p_{n_p(P_q)}, \mathbf{C}), \tag{1}$$

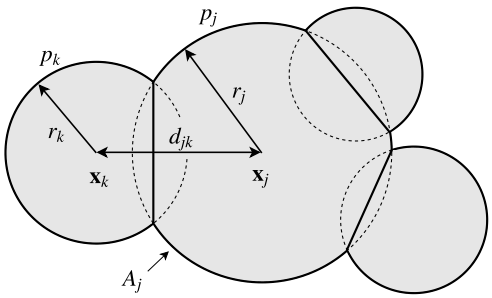

Figure 3: An illustration of the detailed particle model type space showing an aggregate particle composed of primary particles (solid outlines) modelled as overlapping spheres (indicated by dashed lines).

where p_j represents a primary particle and $\mathbf{C}$ is a connectivity matrix tracking which primaries are neighbours [21]. A primary particle p_j is described by

$$p_j = p_j(\eta_j, r_j, \mathbf{x}_j). \tag{2}$$

Each primary particle is characterised by its TiO_2 composition η_j, its radius r_j, and by the position of the primary centre relative to the centre of mass of the aggregate $\mathbf{x}_j$. The degree of overlap between two neighbouring primaries, p_j and p_k, is resolved by their centre to centre separation, $d_{jk} = |\mathbf{x}_j - \mathbf{x}_k|$.

Inception is modelled as a bimolecular collision of two $Ti(OH)_4$ molecules forming a particle consisting of a single primary. The rate is given by the free molecular collision kernel [21]

$$K_{\mathrm{fm}}^{\mathrm{inc}} = \epsilon \sqrt{\frac{\pi k_{\mathrm{B}} T}{m_{\mathrm{Ti(OH)_4}}}} (2 d_{\mathrm{Ti(OH)_4}})^2, \tag{3}$$

with the $Ti(OH)_4$ collision diameter, $d_{\mathrm{Ti(OH)_4}} = 5.128 \times 10^{-10}$ m, calculated from the geometrical parameters calculated by Buerger et al. [35]. The mass of $Ti(OH)_4$ is $m_{\mathrm{Ti(OH)_4}} = 1.925 \times 10^{-25}$ kg and the value for the collision enhancement factor $\epsilon = 2.2$ is taken from previous studies on titania [36, 37].

An aggregate is formed when two particles (single primary or aggregate) stick together as a result of a collision. The rate of coagulation is calculated using a transition kernel [26, 21]

$$K_{\mathrm{tr}} = \left(\frac{1}{K_{\mathrm{sf}}} + \frac{1}{K_{\mathrm{fm}}} \right)^{-1}, \tag{4}$$

where the slip flow and free molecular kernels for particles P_q and P_r are

$$K_{\mathrm{sf}}(P_q, P_r) = \frac{2k_{\mathrm{B}}T}{3\mu}\left(\frac{1+1.257\mathrm{Kn}(P_q)}{d_{\mathrm{c}}(P_q)} + \frac{1+1.257\mathrm{Kn}(P_r)}{d_{\mathrm{c}}(P_r)}\right)(d_{\mathrm{c}}(P_q)+d_{\mathrm{c}}(P_r)) \tag{5}$$

$$K_{\mathrm{fm}}(P_q, P_r) = \epsilon\sqrt{\frac{\pi k_{\mathrm{B}}T}{2}\left(\frac{1}{m(P_q)}+\frac{1}{m(P_r)}\right)}(d_{\mathrm{c}}(P_q)+d_{\mathrm{c}}(P_r))^2\,. \tag{6}$$

m is the aggregate mass, d_{c} is the aggregate collision diameter calculated as per Lavvas et al. [38], μ is the gas-phase viscosity and Kn is the Knudsen number at pressure p and temperature T. The orientations of the colliding particles and point of contact following the collision are determined by ballistic cluster-cluster aggregation with a random impact parameter [39].

A particle may grow via condensation due to a collision between a molecule of $\mathrm{Ti(OH)_4}$ and the particle with the release of two $\mathrm{H_2O}$ molecules. The rate of collision is based on the free molecular kernel and assumes the mass and diameter of the condensing species is much smaller than that of the particle

$$K_{\mathrm{fm}}^{\mathrm{cond}} = \epsilon\sqrt{\frac{\pi k_{\mathrm{B}}T}{2m_{\mathrm{TiO_2}}}}(d_{\mathrm{c}}(P_q))^2. \tag{7}$$

The mass of the condensing species is assumed to be similar to that of $\mathrm{TiO_2}$, $m_{\mathrm{TiO_2}} = 1.323\times10^{-25}$ kg. The condensing mass is added to a constituent primary particle, p_j, selected with probability proportional to its free surface area, A_j, normalised by the free surface area of the aggregate.

Neighbouring primary particles undergo rounding via a sintering process in which the primary centres approach each other increasing their overlap. Mass is conserved by increasing the primary radii. The sintering model follows the approach of Eggersdorfer et al. [34] with the rate for a neck between two primaries evaluated using the grain boundary diffusion model with characteristic time

$$\tau_{\mathrm{s}} = 9.112\times10^{17}Td_{\mathrm{p}}^4\exp\left(\frac{258\ \mathrm{kJ\,mol^{-1}}}{RT}\left(1-\frac{d_{\mathrm{p,crit}}}{d_{\mathrm{p}}}\right)\right)\ \mathrm{s}, \tag{8}$$

where d_{p} is the smaller of the two primary diameters and $d_{\mathrm{p,crit}}$ is the critical sintering diameter that promotes the instantaneous coalescence of primaries with $d_{\mathrm{p}} < d_{\mathrm{p,crit}}$. In our test case we use $d_{\mathrm{p,crit}} = 0$ nm. Once sufficiently sintered, two primaries are assumed to coalesce into a single primary.

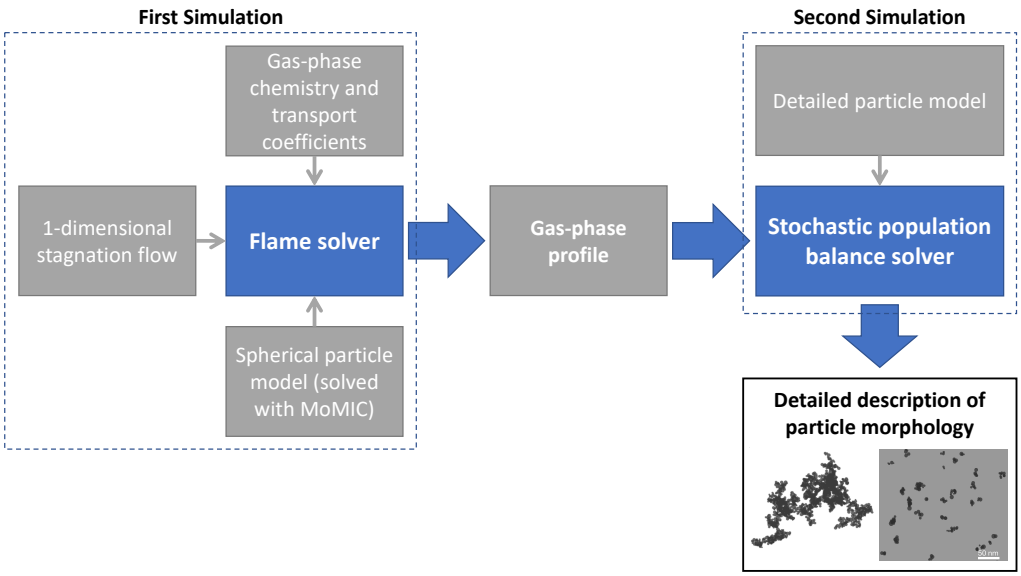

Figure 4: Two-step simulation methodology.

4. Methodology

4.1. Two-step simulation methodology

Figure 4 illustrates the two-step simulation methodology employed. In the first step, the flame is simulated with a one-dimensional stagnation flow approximation, coupled with gas-phase chemistry (Section 3.2) and a spherical particle model (Section 3.3.1) solved with method of moments with interpolative closure (MoMIC). Solving the coupled system to steady state is computationally expensive. MoMIC is chosen because it it numerically simple, easy to couple, less computationally demanding than other moment methods and sufficient to capture the effect of the particles on the gas-phase. This first step is solved as a boundary-value problem using the *k*inetics® software package [40] with the boundary conditions specified according to experimental conditions. The burner-surface separation is 1.06 cm, and the burner and plate temperatures are 423.15 K and 503 K respectively. The exit velocity is 436 cm/s, and species mole fractions of the gas mixture in the nozzle are 3.5% C_2H_4/30% O_2/66.5% Ar (equivalence ratio $\phi = 0.35$) and 580 ppm TTIP, corresponding to a TTIP loading rate of 12 ml/h (this loading rate is used in results hereafter unless otherwise specified). A solution-adapted grid refinement is used in order to achieve convergence with 240–260 grid points. This first step is discussed in detail by Manuputty et al. [8].

In the second step, the resulting gas-phase profile is post-processed with the detailed particle model (Section 3.3.2) to resolve the aggregate particle

morphology, solved using a stochastic numerical method. The flame conditions and gas species are supplied as input to the population balance simulation. The simulation requires the computed profiles to be expressed in terms of the residence time of a Lagrangian particle travelling from the burner to the stagnation plate. The combined convective and thermophoretic velocities are used to calculate the particle time history as per Abid et al. [4].

The stochastic method employs a direct simulation algorithm (DSA) [21] with a majorant kernel and fictitious jumps [41, 26] to improve the computational speed of calculating the coagulation rate, and a linear process deferment algorithm [42] to provide an efficient treatment of sintering and condensation. Simulation results in this study are an average of 4 runs with 8192 stochastic particles.

4.2. Particle population governing equations

4.2.1. First simulation

In the first simulation, the particle population balance is coupled to the flow and gas-phase chemistry through the moment transport equations. This step is discussed in detail by Manuputty et al. [8]. The transport equation for the r^{th}-moment, M_r, is composed of the moment source, advective, thermophoretic and diffusive transport terms [19]

$$\dot{M}_r - \rho u \frac{\mathrm{d}}{\mathrm{d}z}\left(\frac{M_r}{\rho}\right) - \frac{\mathrm{d}}{\mathrm{d}z}\left(v_{\mathrm{T}} M_r\right) + \frac{\mathrm{d}}{\mathrm{d}z}\left(\rho D_{p,1} \frac{\mathrm{d}}{\mathrm{d}z}\left(\frac{M_{r-2/3}}{\rho}\right)\right) = 0, \qquad (9)$$

where ρ is the gas-phase density, v_{T} is the thermophoretic velocity, and u is the convective velocity. $\dot{M}_r$ is the r^{th} moment source term, z is the spatial displacement along the flame and $D_{p,1}$ is the Brownian diffusion coefficient of a TiO_2 monomer. As per Manuputty et al. [8], the thermophoretic velocity and Brownian diffusion coefficient are

$$v_{\mathrm{T}} = -\frac{3}{4}\left(1 + \frac{\pi\alpha_{\mathrm{T}}}{8}\right)^{-1} \frac{\mu}{\rho} \frac{\mathrm{d}\ln T}{\mathrm{d}z}, \qquad (10)$$

$$D_{p,1} = \frac{3}{2\rho}\left(1 + \frac{\pi\alpha_{\mathrm{T}}}{8}\right)^{-1} \sqrt{\frac{\bar{W} k_{\mathrm{B}} T}{2\pi N_{\mathrm{A}}}} \left(\frac{1}{d_1^2}\right), \qquad (11)$$

where the thermal accommodation factor α_{T} is 0.9. $\bar{W}$ is the average molar mass of the gas mixture, k_{B} is the Boltzmann constant, N_{A} is the Avogadro number and μ is the gas-phase viscosity. d_1 is the diameter of a single TiO_2 monomer and is calculated from the bulk density of anatase (3.84 g/cm^3).

4.2.2. Second simulation

In the stochastic simulation, the population balance equations are spatially homogeneous. We consider a Lagrangian description of an ensemble of particles in a sample volume travelling from burner to stagnation plate. The particle ensemble evolves in time with the governing equation:

$$\frac{\mathrm{d}n(x)}{\mathrm{d}t} = R(x) - \gamma n(x), \tag{12}$$

where $n(x)$ is the number density of particles of type x. Here, the type x represents the type-space variables, which for the detailed particle model are given in Eqs. (1) and (2). $R(x)$ is the rate of production of particles of type x: a function of the inception, condensation, coagulation and sintering rates given in Section 3.3.2. γ is the rate of gas-phase expansion: a function of temperature and the rate of production of gas-phase species. The gas-phase conditions in the sample volume (temperature, pressure, and species concentrations) are supplied as input from the first simulation and expressed as a function of the residence time of the Lagrangian sample volume using the combined convective and thermophoretic velocities [4].

The stochastic method approximates real particles with a collection of computational particles in a sample volume V_{smpl}. The sample volume corresponds to the actual volume in the real system in which the number of real particles matches the number of computational particles. γ adjusts the sample volume in response to gas-phase expansion and contraction such that

$$\frac{1}{V_{\mathrm{smpl}}}\frac{\mathrm{d}V_{\mathrm{smpl}}}{\mathrm{d}t} = \gamma. \tag{13}$$

4.2.3. Thermophoretic correction

In order to perform the post-process we need to impose the same conditions on the particle population in the second simulation as modelled in the first. Therefore, the governing equations for both steps of the methodology need to be similar. To compare the governing equations it is convenient to rewrite Eq. (12), the governing equation for the second simulation, in terms of the number density moments, defined as

$$M_r = \sum_{i=1}^{\infty} i^r n_i, \tag{14}$$

where n_i is the number density of aggregate particles containing a total i units of TiO_2. Expressed in terms of the moments the governing equation has the form

$$\frac{\mathrm{d}M_r}{\mathrm{d}t} = \dot{M}_r - \gamma M_r, \tag{15}$$

where $\dot{M}_r$ is the moment source term: a function of the process rates in the second simulation. It is important to note that the moment source in this case is not identical to the moment source term for the first simulation step. This is due to (1) the different particle models used in the two simulations steps, and thus the effect of different particle geometry on process rates, for example, the calculation of the particle collision diameter; and (2) the different treatment of the source terms by the numerical method employed, for example, interpolated closure of fractional order moments by MoMIC. The methodology and analysis here assumes that the source terms are not significantly different.

The equation for the stochastic simulation (Eq. (15)) does not currently account for thermophoretic and diffusive transport. If, however, the thermophoretic and diffusive transport effects in the modelled system are small and can be neglected in the post-process it is straightforward to show that the governing equation in second simulation (Eq. (15)) approximates the moment transport equation solved in the first simulation (Eq. (9)). This is the case for premixed laminar flames with no stagnation plate such as those simulated in Refs. [24, 25, 26, 27, 28]. Neglecting the thermophoretic and diffusive transport terms, the moment transport equation (Eq. (9)) becomes

$$\dot{M}_r - \rho u \frac{\mathrm{d}}{\mathrm{d}z}\left(\frac{M_r}{\rho}\right) = 0. \tag{16}$$

Expressing Eq. (16) in terms of the residence time of a Langrangian particle by making the coordinate transformation $\mathrm{d}z = u\,\mathrm{d}t$ yields the equation for the second simulation (Eq. (15)) with a gas-phase expansion rate

$$\gamma = -\frac{1}{\rho}\frac{\mathrm{d}\rho}{\mathrm{d}t}. \tag{17}$$

Here, the sample volume adjustment corresponds to the change in gas-phase density i.e. the gas-phase mass contained within the sample volume is conserved (mass transfer to the particle phase is assumed to be negligible).

In the case of a stagnation flame, as modelled in this work, thermophoresis is significant near the cooled stagnation plate due to a steep temperature gradient, so the thermophoretic transport term cannot be neglected. Assuming instead that only the diffusive term is negligible Eq. (9) becomes

$$\dot{M}_r - (u + v_\mathrm{T})\frac{\mathrm{d}M_r}{\mathrm{d}z} + \left(\frac{u}{\rho}\frac{\mathrm{d}\rho}{\mathrm{d}z} - \frac{\mathrm{d}v_\mathrm{T}}{\mathrm{d}z}\right) M_r = 0, \tag{18}$$

Using the convective and thermophoretic velocities, we make the coordinate transformation $\mathrm{d}z = (u + v_\mathrm{T})\,\mathrm{d}t$ to express Eq. (18) in terms of the residence

time of a Lagrangian particle

$$\dot{M}_r - \frac{\mathrm{d}M_r}{\mathrm{d}t} + \frac{1}{u + v_\mathrm{T}} \left(\frac{u}{\rho} \frac{\mathrm{d}\rho}{\mathrm{d}t} - \frac{\mathrm{d}v_\mathrm{T}}{\mathrm{d}t} \right) M_r = 0, \tag{19}$$

which has the form of the governing equation for the second simulation (Eq. (15)) with

$$\gamma = -\frac{1}{(u + v_\mathrm{T})} \left(\frac{u}{\rho} \frac{\mathrm{d}\rho}{\mathrm{d}t} - \frac{\mathrm{d}v_\mathrm{T}}{\mathrm{d}t} \right). \tag{20}$$

Thus, the effect of thermophoresis is now accounted for in the volume adjustment term in the stochastic population balance where the convective and thermophoretic velocities, and gas-phase density are supplied as input. Note that setting $v_\mathrm{T} = 0$ returns the earlier relation (Eq. (17)).

The diffusive term cannot be dealt with in the same way because it is a second order derivative of the moments and not independent of the PSD. A possible method could be to apply a diffusion correction to the reactor volume for a specific moment order. For example, applying the correction for $r = 1$ to ensure the system mass remains in agreement between the two simulations. However, the correction would only be approximate for other moments and is outside the scope of this work.

4.3. Simulated TEM images

The individual primary particle coordinate information tracked in the detailed type-space allows for visualisation of simulated particles. In particular, TEM-style images can be generated by sampling the particle ensemble. Such images can then be compared with experimental TEM micrographs. A TEM-style image is produced using the following algorithm:

1. Uniformly select a particle P_q.
2. Rotate P_q to a random orientation using the method described by Arvo [43].
3. Generate (x, y) coordinates uniformly in the image plane with $-a \leq x \leq a$ and $-b \leq y \leq b$, where a and b define the frame size.
4. Position P_q above the image plane with its centre of mass at (x, y).
5. Project P_q down onto the image plane.
6. Repeat steps 1–5 for further particles.

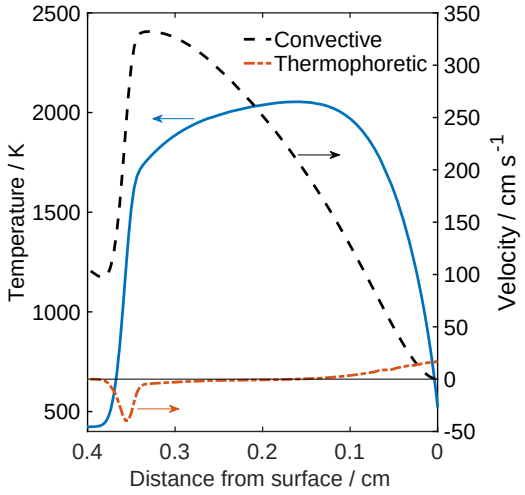

Figure 5: Temperature and velocity profiles obtained from the first simulation.

5. Results and Discussion

5.1. Transport terms

Figure 5 shows the simulated temperature and velocity profiles obtained from the first step. We observe two regions with significant thermophoresis: at the flame front where the temperature increases steeply; and near the cooled stagnation plate where the temperature rapidly decreases. The region near the stagnation surface is of particular significance because the convective velocity is low, so in the Lagrangian view a particle will spend a large fraction of its residence time here. It is therefore important to correctly account for the effect of transport processes on the particle population dynamics in this region.

In Fig. 6 we compare the relative sizes of the individual terms in moment transport equation (Eq.(9)) solved in the first simulation step. The advective, thermophoretic, diffusive, and moment source terms are shown for the first three moments $r = 0, 1, 2$. The plots show that for a stagnation flame the transport terms are significant and need to be considered in the second step post-process. In particular, the thermophoretic term dominates in the region near the stagnation surface for the higher order moments, and will influence the PSD near the point of experimental measurement.

Diffusion is much less significant at the stagnation surface and can be assumed to be negligible here. However, at the flame front the diffusive term is non-negligible, particularly in the zeroth moment. Here, the convective velocity is very high so in the Lagrangian view diffusive effects will occur over

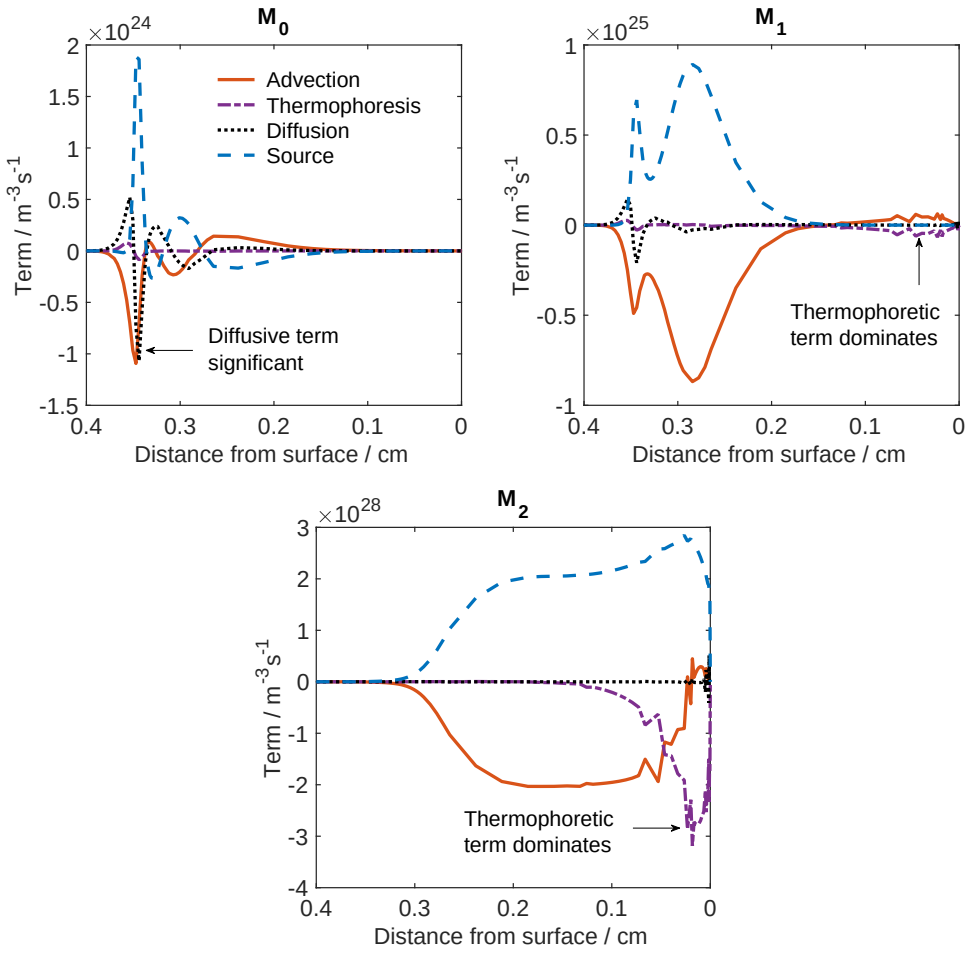

Figure 6: Moment transport equation terms from the first simulation.

a short period of time early in the evolution of the particle population; thus, the impact of diffusion on the final PSD is likely to be much less significant than thermophoresis.

5.2. Post-processing method evaluation

Evaluation of the post-processing methodology is necessary to ensure that meaningful results are obtained from the post-processing step; specifically, that the particle population evolves under similar conditions in the post-process as modelled in the first simulation. We can evaluate the effect of applying the thermophoretic correction (Eq. (20)) to the second step simulation by post-processing the flame profile with the spherical particle model and comparing the results of the post-process with the moments calculated in the first simulation. Using the same particle model in both simulation steps

eliminates particle model dependent effects on the solutions. Therefore, any differences in the moments obtained from the first and second simulations are either due to (1) the treatment of transport in the governing equations or (2) assumptions and approximations made in the numerical methods used to solve the governing equations. For the purpose of comparison, the moments solved by MoMIC in the first simulation are treated as the reference solution because this is the fully coupled simulation solved with transport.

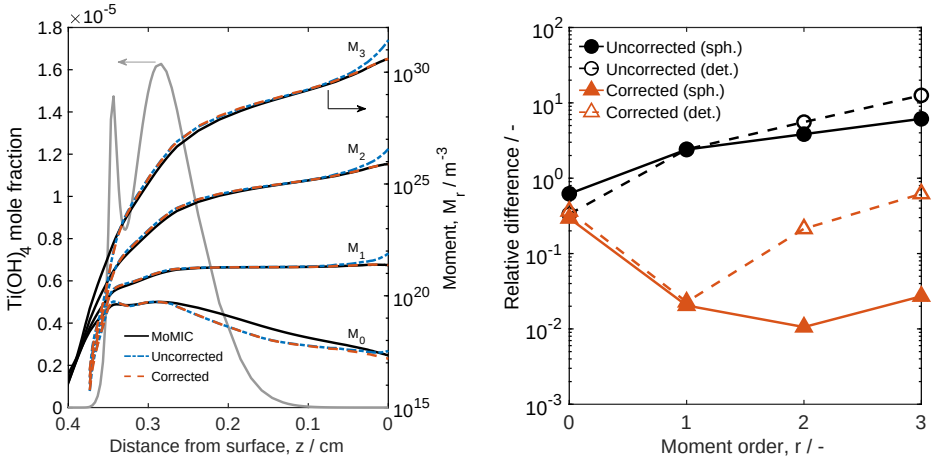

Figure 7: (a) Moments obtained from the first-step MoMIC simulation and from post-processing with a spherical particle model with and without the thermophoretic correction. The $Ti(OH)_4$ collision species mole fraction is added for reference. (b) The relative difference in the moments at the stagnation surface measured against the MoMIC solution for the spherical (sph.) and detailed (det.) particle models.

Figure 7(a) shows the moments obtained by post-processing using the spherical particle model with and without thermophoretic correction, together with the MoMIC reference solution. The $Ti(OH)_4$ collision species mole fraction is included for reference. The thermophoretic correction was found to significantly improve the agreement between the post-process and the MoMIC reference solution near the stagnation surface (at $z = 0$ cm) where thermophoretic transport effects are most significant.

The large difference in the predicted moments at the flame front is a consequence of the resolution of stochastic method. A statistically significant solution only exists once the concentration of $Ti(OH)_4$, the collision species, is high enough and therefore the particle inception rate is large enough for particles to be incepted into the simulation sample volume with reasonable probability.

The relative difference in the moments predicted by the post-process at the stagnation surface measured against the MoMIC reference solution is plotted as a function of moment order, r, in Fig. 7(b). Results from post-processing with the spherical and detailed particle model are shown, with and without thermophoretic correction. For $r \geq 1$ a significant reduction in the relative difference is observed with the introduction of the thermophoretic correction for both particle models. Naturally, the spherical particle model shows better agreement (for $r \geq 2$) than the detailed model because a spherical model is also used in the first simulation. The aggregate particle structure described by the detailed model is expected to affect the shape of the predicted PSD, and thus, the higher order moments.

The zeroth moment shows little to no improvement when the thermophoretic correction is introduced. Two possible reasons for this are: the greater relative importance of diffusion on M_0 (Fig. 6); and differences in the numerical methods, especially in the treatment of coagulation. A difference between the two solutions is expected because MoMIC introduces a numerical approximation, while the stochastic method treats coagulation exactly. In particular, the MoMIC calculation of the M_0 source term requires an extrapolated negative order fractional moment [44], which is prone to numerical error. Furthermore, the divergence in M_0 in Fig. 7(a) does not coincide with extrema in the M_0 diffusion term in Fig. 6 suggesting that diffusion is not the cause. At the point of divergence the M_0 diffusion term is negligible. This would suggest that the error arises from differences between the two numerical methods.

Figure 8 shows a comparison of the average particle diameter as a function of TTIP loading for spherical and detailed particle models, with and without the thermophoretic correction. For the detailed particle model the collision diameter is calculated as per Lavvas et al. [38]. We see that the thermophoretic correction reduces the error substantially for both spherical and detailed models. However, the difference observed in the zeroth moment in Fig. 7 is carried over into the average particle properties, hence the agreement is not as good as for the individual moments. The plots show a general trend of improving agreement with increased TTIP loading. This is primarily driven by the behaviour of the divergence in M_0 and not an effect of the thermophoretic correction.

The methodology considers two-way coupling between the gas and particle phases only in the first simulation step. The assumption is that the spherical particle model employed in the first simulation provides a reasonable approximation of particle morphology when coupling to the gas-phase is most important. Non-spherical particles would give different process rates for gas-phase interactions due to different particle morphology affecting properties such as the collision diameter and free surface area. The mole fraction

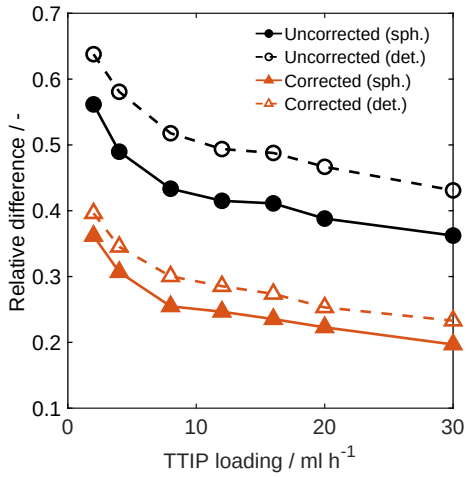

Figure 8: Relative difference in particle collision diameter measured against the MoMIC reference solution plotted as a function of TTIP loading. Results from post-processing using a spherical particle model (sph.) and detailed particle model (det.) are shown with and without thermophoretic correction.

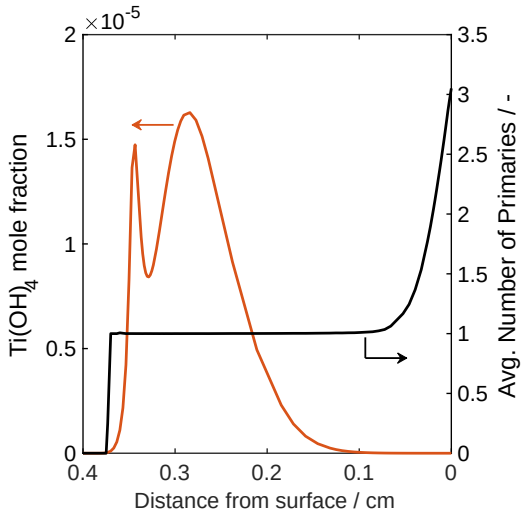

Figure 9: Mole fraction of $Ti(OH)_4$, the collision species, and the average number of primaries per particle as a function of distance from the stagnation surface.

of the gas-phase collision species ($Ti(OH)_4$) obtained from the first simulation and the average number of primaries per particle predicted by the post-process are plotted in Fig. 9 as function of the distance from the stagnation surface. We observe that the collision species is exhausted prior to the formation of aggregates suggesting that a spherical particle model provides

a reasonable description of particle morphology when $Ti(OH)_4$ is being consumed from the gas-phase and two-way coupling is most important. Particles remain spherical in this high temperature region due to rapid coalescence of colliding particles. The detailed model predicts aggregate formation only after the particle processes have effectively decoupled from the gas-phase chemistry.

5.3. Evolution of aggregate particle morphology

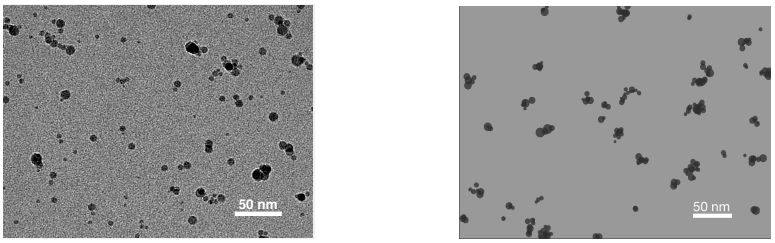

(a) (b)

Figure 10: (a) An experimental TEM image (unpublished data) and (b) a simulated TEM-style image.

Figure 10 shows an experimental TEM image of aggregate TiO_2 particles synthesised in a stagnation flame and a simulated TEM-style image produced under similar modelled conditions. In both images we observe sintered aggregate particles of comparable aggregate and primary size. This illustrates that resolving the aggregate structure and modelling morphology dependent processes such as sintering are important for making proper comparison with experimental results.

In Fig. 11 the average number of primaries per aggregate predicted by the post-process as a function of distance from the stagnation plate is plotted together with the simulated temperature profile. The formation of aggregates is observed as the temperature decreases substantially near the stagnation surface. This is due to the rate of sintering having a stronger temperature dependence than coagulation. The TEM-style snapshots generated at different points along the flame illustrate this change in particle morphology.

5.4. Comparison with experimental PSD

In this section we use the methodology presented in this paper to simulate the premixed stagnation flame experiment of Tolmachoff et al. [2] using a detailed particle model. The experiment has been previously simulated by Manuputty et al. [8] using a single step TTIP decomposition model with the overall rate given by Okuyama et al. [45]. In this work, we simulate

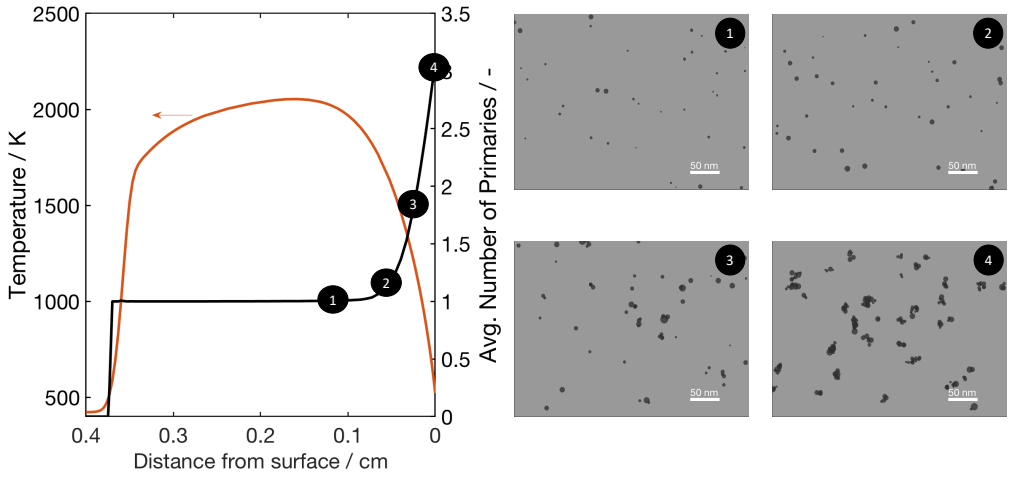

Figure 11: Simulated temperature profile and average number of primaries per aggregate predicted by the post-process. Four simulated TEM-style snapshots are shown at different points along the flame.

the experiment using the gas-phase chemistry described in Section 3.2 and collision limited inception and condensation reactions with $Ti(OH)_4$ as the collision species as described in Sections 3.3.1 and 3.3.2. Otherwise, the details of the modelled burner configuration and first simulation step are the same as in Ref. [8].

In the experimental investigation by Tolmachoff et al. [2] a TTIP-doped premixed laminar flame (3.96% C_2H_4/26.53% O_2/ Ar, $\phi = 0.45$) issued from an aerodynamically shaped nozzle impinges on a rotating stagnation plate. In the present analysis, as in the previous modelling work performed by Manuputty et al. [8], it is important to consider two aspects of this burner configuration: the stagnation surface temperature and the particle sampling technique.

Cooling jets and convection maintained the stagnation plate temperature at $T_s \sim 400$ K for rotational speeds in the range of 100–600 RPM. Without rotation, the absence of convective cooling increased the plate temperature as high as $T_s \sim 1000$ K. As per Ref. [8] other effects of rotation are not considered here. Tolmachoff et al. [2] suggest that rotation results in little to no change in flame characteristics due to the thin boudary layer, hence it is reasonable to only vary the stagnation plate temperature.

Two different particle sampling techniques were used in the experimental study: a scanning mobility particle sizer (SMPS) with sampling probe

mounted in the plate was used for the non-rotating plate; while TEM image analysis was performed on particles collected by rapid insertion of a TEM grid fastened to the plate when the plate was rotating.

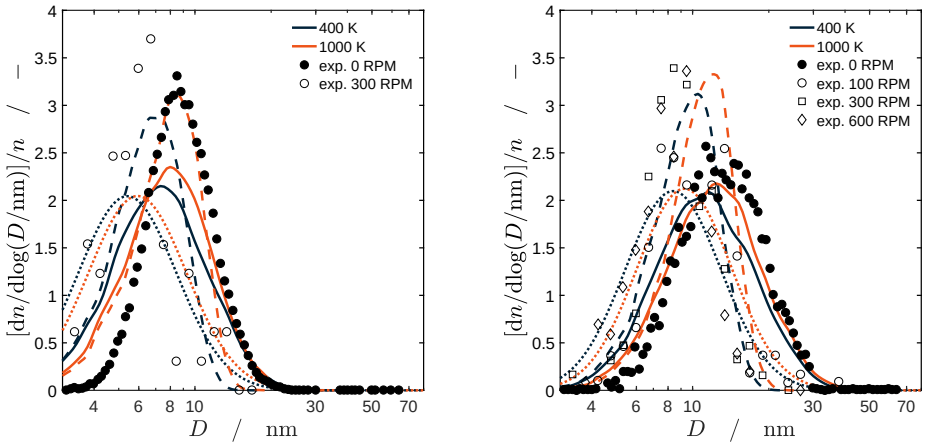

Figure 12: Particle size distributions of TiO_2 produced at (a) 306 ppm and (b) 1070 ppm TTIP loadings. Symbols: experimental data from Tolmachoff et al. [2, Fig. 8]; Solid lines: collision diameter distribution; Dashed lines: primary particle size distribution; Dotted lines: log-normal PSD from MoMIC results. Simulation results are presented for stagnation plate temperatures of 400 K and 1000 K.

Simulations were performed using a collision enhancement factor of $\epsilon = 2.64$ as per Manuputty et al. [8], and a critical sintering diameter of $d_{\mathrm{p,crit}} = 2$ nm. Other model parameters are as given in Section 3.3.2. $d_{\mathrm{p,crit}} = 2$ nm was found to give the best fit of the right tail of the simulated collision diameter distribution to the 0 RPM experimental case. This value is consistent with the molecular dynamics study of Buesser et al. [46], who found that small primaries with $d_{\mathrm{p}} < 4$ nm sinter significantly faster than rates predicted by models developed for larger particles.

Figure 12 shows the simulated particle size distributions for two different TTIP loadings (306 ppm and 1070 ppm) with the two different plate temperatures (400 K for the rotating plate and 1000 K for the stationary plate). Gaussian kernel density estimates are plotted for the collision diameter and primary particle diameter distributions obtained from the detailed model post-process. Log-normal distributions were generated from the first simulation step MoMIC data with median particle diameter and geometric

standard deviation calculated as per Manuputty et al. [8]

$$\langle D_{\mathrm{p}} \rangle = \frac{d_1 \mu_{1/3}}{\sqrt{1 + \frac{\mu_{2/3} - \mu_{1/3}^2}{\mu_{1/3}^2}}} \tag{21}$$

$$\mathrm{GSD} = \exp \sqrt{\ln \left(1 + \frac{\mu_{2/3} - \mu_{1/3}^2}{\mu_{1/3}^2} \right)}, \tag{22}$$

where μ_r are the fractional reduced moments. The experimental data are from Tolmachoff et al. [2, Fig. 8].

Our simulations predict a small degree of aggregate formation indicated by the differing collision diameter and primary diameter distributions; notably the position of the respective right hand tails of each distribution. We begin by comparing the aggregate collision diameter distribution for stagnation temperature $T_{\mathrm{s}} = 1000$ K (solid red lines) with the 0 RPM SMPS data (solid symbols) because the instrument measures the aggregate particle size. The 1070 ppm loading case shows excellent agreement with the experimental data of Tolmachoff et al. [2]. For the lower loading 306 ppm case, however, our simulation predicts a broader distribution compared to the experimental results. It is worth noting that we are comparing our modelled collision diameter with SMPS measured mobility diameter and the two are unlikely to be identical measures of particle size, which may contribute to some of the observed differences.

To compare our simulations with the rotating disc experimental data we use the primary diameter distribution. In the experimental study [2] measurements of particle size for the rotating disc were performed using TEM image analysis, in which case the diameters of individual primaries were measured. Thus, we compare the primary diameter distribution for $T_{\mathrm{s}} = 400$ K (dashed blue line) with the experimental results with rotation (open symbols). The agreement with the experimental data is reasonably good in both cases; although the simulated median size is slightly larger and the distribution is shifted to the right. On the other hand, the aggregate collision diameter distributions (solid blue lines) are broader and extend to larger particle sizes. Tolmachoff et al. [2] attribute the difference in the rotating vs. non-rotating disc PSDs to the change in disc temperature rather than measurement technique, supported by an earlier study showing that diameters measured by SMPS agree with those measured by TEM analysis in the size range of interest [47]. In contrast, our simulation results suggest that while some of the difference can be attributed to the stagnation surface temperatures it is also possible that a small degree of aggregation can result in

different measured distributions. In this case the mean number of primaries per aggregate was $\bar{n}_{\mathrm{p}} < 2$ for all simulations.

It is also worth comparing the detailed model simulation results with the log-normal distributions obtained from the first step MoMIC simulations (dotted lines) with spherical particle assumption. The MoMIC results underpredict the median size for the non-rotating (0 RPM, $T_{\mathrm{s}} = 1000$ K) disc (dotted red lines vs. solid symbols) while the rotating case ($T_{\mathrm{s}} = 400$ K) is in better agreement (dotted blue lines vs. open symbols), likely because of the spherical particle assumption. This would suggest that a simple spherical particle model is not sufficient and a detailed particle description is needed to model the system and provide additional insight.

6. Conclusions

This paper presented a general two-step modelling methodology able to resolve the complex aggregate morphology of nanoparticles synthesised in a stagnation flame. The methodology was applied to the combustion synthesis of TiO_2 particles from TTIP precursor. A detailed particle model is necessary to simulate the evolution of aggregate particles observed in experiments.

The first step of the two-step methodology couples detailed gas-phase chemistry, a one-dimensional flow model and spherical particle model solved with MoMIC. The resulting flame profile is then post-processed using a detailed particle model capable of tracking individual primary coordinates to resolve the aggregate structure. The method allows for comparison with experimental observations such as TEM images and enables the study of morphology dependent particle processes.

Examination of the magnitude of the terms in the MoMIC equations showed that thermophoretic transport effects are significant near the stagnation surface and must be accounted for in the second step where the flame profile is post-processed. To do this, a thermophoretic correction to the simulation sample volume was introduced. Comparison of moments predicted by the second-step post-process against the first-step MoMIC solution showed that the thermophoretic correction leads to a significant reduction in the error associated with the post-process. However, a divergence in the zeroth moment was observed, which has an impact on the average particle properties. This is suspected to be caused by differences between the two numerical methods used; in particular, their treatment of coagulation.

The stagnation flame experiment of Tolmachoff et al. [2] was simulated using the two-step methodology with detailed particle model to demonstrate the ability of a detailed description of particles to provide additional insight and explain experimental observations. The detailed model was better able to

reproduce the measured PSDs compared to a simple spherical particle model. While the model itself was not the subject of this paper, the methodology presented here allows it to be applied to a widely used class of flame, and thus provides a means to evaluate the model against experimental data such as aggregate size, primary size and primary number distributions. This will be the subject of future work.

Acknowledgements

This project is supported by the National Research Foundation (NRF), Prime Minister's Office, Singapore under its Campus for Research Excellence and Technological Enterprise (CREATE) programme. The authors also thank Venator and CMCL Innovations for generous financial support.

References

[1] B. Zhao, K. Uchikawa, J. R. McCormick, C. Y. Ni, J. G. Chen, H. Wang, Ultrafine anatase TiO_2 nanoparticles produced in premixed ethylene stagnation flame at 1 atm, Proc. Combust. Inst. 30 (2005) 2569–2576, doi:10.1016/j.proci.2004.08.146.

[2] E. D. Tolmachoff, A. D. Abid, D. J. Phares, C. S. Campbell, H. Wang, Synthesis of nano-phase TiO_2 crystalline films over premixed stagnation flames, Proc. Combust. Inst. 32 (2009) 1839–1845, doi:10.1016/j.proci.2008.06.052.

[3] S. Memarzadeh, E. D. Tolmachoff, D. J. Phares, H. Wang, Properties of nanocrystalline TiO_2 synthesized in premixed flames stabilized on a rotating surface, Proc. Combust. Inst. 33 (2011) 1917–1924, doi:10.1016/j.proci.2010.05.065.

[4] A. D. Abid, J. Camacho, D. A. Sheen, H. Wang, Quantitative measurement of soot particle size distribution in premixed flames - The burner-stabilized stagnation flame approach, Combust. Flame 156 (2009) 1862–1870, doi:10.1016/j.combustflame.2009.05.010.

[5] J. Camacho, C. Liu, C. Gu, H. Lin, Z. Huang, Q. Tang, X. You, C. Saggese, Y. Li, H. Jung, L. Deng, I. Wlokas, H. Wang, Mobility size and mass of nascent soot particles in a benchmark premixed ethylene flame, Combust. Flame 162 (2015) 3810–3822, doi:10.1016/j.combustflame.2015.07.018.

[6] J. I. Jeong, M. Choi, A bimodal moment model for the simulation of particle growth, J. Aerosol Sci. 35 (2004) 1071–1090, doi: 10.1016/j.jaerosci.2004.04.005.

[7] Y. Sung, V. Raman, H. Koo, M. Mehta, R. O. Fox, Large-eddy simulation modeling of turbulent flame synthesis of titania nanoparticles using a bivariate particle description, AIChE J. 60 (2014) 459–472, doi: 10.1002/aic.14279.

[8] M. Y. Manuputty, J. Akroyd, S. Mosbach, M. Kraft, Modelling TiO_2 formation in a stagnation flame using method of moments with interpolative closure, Combust. Flame 178 (2017) 135–147, doi: 10.1016/j.combustflame.2017.01.005.

[9] Y. Xiong, S. E. Pratsinis, Formation of agglomerate particles by coagulation and sintering–Part I. A two-dimensional solution of the population balance equation, J. Aerosol Sci. 24 (1993) 283–300, doi:10.1016/0021-8502(93)90003-R.

[10] K. Nakaso, T. Fujimoto, T. Seto, M. Shimada, K. Okuyama, M. M. Lunden, Size distribution change of titania nano-particle agglomerates generated by gas phase reaction, agglomeration, and sintering, Aerosol Sci. Technol. 35 (2001) 929–947, doi:10.1080/02786820126857.

[11] S. Tsantilis, H. K. Kammler, S. E. Pratsinis, Population balance modeling of flame synthesis of titania nanoparticles, Chem. Eng. Sci. 57 (2002) 2139–2156, doi:10.1016/S0009-2509(02)00107-0.

[12] S. Tsantilis, S. E. Pratsinis, Narrowing the size distribution of aerosol-made titania by surface growth and coagulation, J. Aerosol Sci. 35 (2004) 405–420, doi:10.1016/j.jaerosci.2003.09.006.

[13] M. C. Heine, S. E. Pratsinis, Polydispersity of primary particles in agglomerates made by coagulation and sintering, J. Aerosol Sci. 38 (2007) 17–38, doi:10.1016/j.jaerosci.2006.09.005.

[14] D. L. Wright, R. McGraw, D. E. Rosner, Bivariate extension of the quadrature method of moments for modeling simultaneous coagulation and sintering of particle populations, J. Colloid Interface Sci. 236 (2001) 242–251, doi:10.1006/jcis.2000.7409.

[15] D. L. Marchisio, R. O. Fox, Solution of population balance equations using the direct quadrature method of moments, J. Aerosol Sci. 36 (2005) 43–73, doi:10.1016/j.jaerosci.2004.07.009.

[16] M. E. Mueller, G. Blanquart, H. Pitsch, A joint volume-surface model of soot aggregation with the method of moments, Proc. Combust. Inst. 32 (2009) 785–792, doi:10.1016/j.proci.2008.06.207.

[17] M. E. Mueller, G. Blanquart, H. Pitsch, Hybrid Method of Moments for modeling soot formation and growth, Combust. Flame 156 (2009) 1143–1155, doi:10.1016/j.combustflame.2009.01.025.

[18] W. J. Menz, M. Kraft, The suitability of particle models in capturing aggregate structure and polydispersity, Aerosol Sci. Technol. 47 (2013) 734–745, doi:10.1080/02786826.2013.788244.

[19] E. K. Y. Yapp, D. Chen, J. Akroyd, S. Mosbach, M. Kraft, J. Camacho, H. Wang, Numerical simulation and parametric sensitivity study of particle size distributions in a burner-stabilised stagnation flame, Combust. Flame 162 (2015) 2569–2581, doi:10.1016/j.combustflame.2015.03.006.

[20] W. J. Menz, M. Kraft, A new model for silicon nanoparticle synthesis, Combust. Flame 160 (2013) 947–958, doi:10.1016/j.combustflame.2013.01.014.

[21] S. Shekar, W. J. Menz, A. J. Smith, M. Kraft, W. Wagner, On a multivariate population balance model to describe the structure and composition of silica nanoparticles, Comput. Chem. Eng. 43 (2012) 130–147, doi:10.1016/j.compchemeng.2012.04.010.

[22] A. Boje, J. Akroyd, S. Sutcliffe, J. Edwards, M. Kraft, Detailed population balance modelling of TiO_2 synthesis in an industrial reactor, Chem. Eng. Sci. 164 (2017) 219–231, doi:10.1016/j.ces.2017.02.019.

[23] C. Lindberg, J. Akroyd, M. Kraft, Developing breakage models relating morphological data to the milling behaviour of flame synthesised titania particles, Chem. Eng. Sci. 166 (2017) 53–65, doi:10.1016/j.ces.2017.03.016.

[24] M. Balthasar, M. Kraft, A stochastic approach to calculate the particle size distribution function of soot particles in laminar premixed flames, Combust. Flame 133 (2003) 289 – 298, doi:10.1016/S0010-2180(03)00003-8.

[25] J. Singh, M. Balthasar, M. Kraft, W. Wagner, Stochastic modeling of soot particle size and age distributions in laminar premixed flames, Proc. Combust. Inst. 30 (2005) 1457 – 1465, doi:10.1016/j.proci.2004.08.120.

[26] R. I. A. Patterson, J. Singh, M. Balthasar, M. Kraft, W. Wagner, Extending stochastic soot simulation to higher pressures, Combust. Flame 145 (2006) 638–642, doi:10.1016/j.combustflame.2006.02.005.

[27] N. Morgan, M. Kraft, M. Balthasar, D. Wong, M. Frenklach, P. Mitchell, Numerical simulations of soot aggregation in premixed laminar flames, Proc. Combust. Inst. 31 (2007) 693 – 700, doi:10.1016/j.proci.2006.08.021.

[28] D. Chen, Z. Zainuddin, E. Yapp, J. Akroyd, S. Mosbach, M. Kraft, A fully coupled simulation of PAH and soot growth with a population balance model, Proc. Combust. Inst. 34 (2013) 1827 – 1835, doi:10.1016/j.proci.2012.06.089.

[29] J. Camacho, A. V. Singh, W. Wang, R. Shan, E. K. Y. Yapp, D. Chen, M. Kraft, H. Wang, Soot particle size distributions in premixed stretch-stabilized flat ethylene-oxygen-argon flames, Proc. Combust. Inst. 36 (2017) 1001–1009, doi:10.1016/j.proci.2016.06.170.

[30] H. Wang, X. You, A. V. Joshi, S. G. Davis, A. Laskin, F. Egolfopoulos, C. K. Law, USC mech version II. High-temperature combustion reaction model of H_2/CO/C_1-C_4 compounds, URL `http://ignis.usc.edu/USC_Mech_II.htm`, accessed on 12 December 2015, 2007.

[31] P. Buerger, D. Nurkowski, J. Akroyd, M. Kraft, A kinetic mechanism for the thermal decomposition of titanium tetraisopropoxide, Proc. Combust. Inst. 36 (2017) 1019–1027, doi:10.1016/j.proci.2016.08.062.

[32] M. Kraft, Modelling of particulate processes, KONA Powder Part. J. 23 (2005) 18–35, doi:10.14356/kona.2005007.

[33] M. L. Eggersdorfer, D. Kadau, H. J. Herrmann, S. E. Pratsinis, Multiparticle sintering dynamics: From fractal-like aggregates to compact structures, Langmuir 27 (2011) 6358–6367, doi:10.1021/la200546g.

[34] M. L. Eggersdorfer, D. Kadau, H. J. Herrmann, S. E. Pratsinis, Aggregate morphology evolution by sintering: Number and diameter of primary particles, J. Aerosol Sci. 46 (2012) 7–19, doi:10.1016/j.jaerosci.2011.11.005.

[35] P. Buerger, D. Nurkowski, J. Akroyd, S. Mosbach, M. Kraft, First-principles thermochemistry for the thermal decomposition of titanium tetraisopropoxide, J. Phys. Chem. A 119 (2015) 8376–8387, doi:10.1021/acs.jpca.5b01721.

[36] J. Akroyd, A. J. Smith, R. Shirley, L. R. McGlashan, M. Kraft, A coupled CFD-population balance approach for nanoparticle synthesis in turbulent reacting flows, Chem. Eng. Sci. 66 (2011) 3792–3805, doi: 10.1016/j.ces.2011.05.006.

[37] R. H. West, R. Shirley, M. Kraft, C. F. Goldsmith, W. H. Green, A detailed kinetic model for combustion synthesis of titania from $TiCl_4$, Combust. Flame 156 (2009) 1764–1770, doi: 10.1016/j.combustflame.2009.04.011.

[38] P. Lavvas, M. Sander, M. Kraft, H. Imanaka, Surface chemistry and particle shape. Processes for the evolution of aerosols in Titan's atmosphere, Astrophys. J. 728 (2011) 80, doi:10.1088/0004-637X/728/2/80.

[39] R. Jullien, Transparency effects in cluster-cluster aggregation with linear trajectories, J. Phys. A: Math. Gen. 17 (1984) L771–L776, doi: 10.1088/0305-4470/17/14/009.

[40] CMCL Innovations, *k*inetics®, URL `http://www.cmclinnovations.com/`, 2016.

[41] M. Goodson, M. Kraft, An efficient stochastic algorithm for simulating nano-particle dynamics, J. Comput. Phys. 183 (2002) 210–232, doi: 10.1006/jcph.2002.7192.

[42] R. I. A. Patterson, J. Singh, M. Balthasar, M. Kraft, J. R. Norris, The linear process deferment algorithm: A new technique for solving population balance equations, SIAM J. Sci. Comput. 28 (2006) 303–320, doi:10.1137/040618953.

[43] J. Arvo, Fast random rotation matrices, in: D. Kirk (Ed.), Graphics Gems III, Academic Press, 117–120, 1992.

[44] M. Frenklach, Method of moments with interpolative closure, Chem. Eng. Sci. 57 (2002) 2229 – 2239, doi:10.1016/S0009-2509(02)00113-6.

[45] K. Okuyama, R. Ushio, Y. Kousaka, R. C. Flagan, J. H. Seinfeld, Particle generation in a chemical vapor deposition process with seed particles, AIChE J. 36 (1990) 409–419, doi:10.1002/aic.690360310.

[46] B. Buesser, A. J. Gröhn, S. E. Pratsinis, Sintering rate and mechanism of TiO_2 nanoparticles by molecular dynamics, J. Phys. Chem. C 115 (2011) 11030–11035, doi:10.1021/jp2032302.

[47] B. Zhao, K. Uchikawa, H. Wang, A comparative study of nanoparticles in premixed flames by scanning mobility particle sizer, small angle neutron scattering, and transmission electron microscopy, Proc. Combust. Inst. 31 (2007) 851–860, doi:10.1016/j.proci.2006.08.064.

10b-sim-tem-12mlh.png

Click here to download LaTeX Source Files: 10b-sim-TEM-12mlh.png

11-evolution.pdf

Click here to download LaTeX Source Files: 11-evolution.pdf

12a-306ppm-psd.pdf

Click here to download LaTeX Source Files: 12a-306ppm-PSD.pdf

12b-1070ppm-psd.pdf

Click here to download LaTeX Source Files: 12b-1070ppm-PSD.pdf